Dynamics of Flexible Solar Updraft Towers

by

Michael Chi

A thesis submitted in partial fulfillment of the requirements for the degree of

Master of Science

in

Applied Mathematics

Department of Mathematical and Statistical Sciences

University of Alberta

Abstract

Solar updraft towers offers a simple and alternative method of generating electricity. However, it is unclear on how to build a tall, free standing structure that can withstand the unpredictable and destructive force of the wind. A tower consisting of stacked inflatable toroidal elements have been suggested and the dynamics of the tower will be analyzed. Using Lagrangian reduction by symmetry, the theory for the 3D motion for the tower is developed. By confining the motion to two-dimensions, numerical simulations are performed to study the tower's stability and is compared with the data collected from a experimental prototype showing good agreement with theoretical results.

Preface

Research of the thesis in Chapters 2-4 has been performed in collaboration with Dr. V Putkaradze from the University of Alberta, and Dr. F Gay-Balmaz from Ecole Normale Supérieure de Paris. Experimental data in Chapter 5 was collected by Dr. P Vorobieff. Chapters 2-5 have been submitted for publication. My work includes verifying the equations in Chapters 2-4 and computation of some numerical simulations in Chapter 5.

Acknowledgements

First, I would like to express my deep gratitude to Dr. Vakhtang Putkaradze for his support and guidance in my research. His helpful suggestions and advice has helped me enormously in writing my thesis. It has been a great pleasure to work under his supervision.

I would also like to thank my fellow colleagues Patrick Conner and Travis Boblin for their support throughout my graduate studies. It has been a tough, yet exciting experience but their encouragement has kept me going and I am truly grateful for such wonderful friends.

Lastly, I would like to thank all the students and professors that made an impact in my graduate career at the University of Alberta. All the lasting memories will be cherished forever.

Table of Contents

List of Tables

List of Figures

Chapter 1

Introduction

Solar updraft towers provide an alternative for generating electricity from solar radiation. The main idea behind the production of energy is quite simple. The air within a collector (greenhouse) is heated from solar radiation. The warmer air then escapes through a tall pipe which connects the hot volume of the collector with the cooler air above the ground. The temperature difference induces convection which turns a turbine within the pipe and generates electricity. As a comparison to the traditional photovoltaic (PV) cells, one advantage of the solar towers is the operation of the tower during both the day and the night. The continual temperature difference between the collector and the pipe due to the thermal mass beneath the ground allows the tower to operate whereas the PV cells are only optimal during the peak of the day. Another advantage over most conventional power stations, such as coal or nuclear power plants, is that the solar towers do not require cooling water. This is especially beneficial for countries where the water supply is demanding. Although the concepts and ideas behind solar towers seem quite feasible, it is important to consider both the costs to build and maintain the

towers as well as the efficiency. One of the ways to improve the efficiency is to increase the temperature differential between the greenhouse on the bottom and the exhaust at the top. This can be achieved by building a taller tower, however, this would increase the material costs to construct the tower and maintenance can be challenging for a larger tower. These factors must be taken into consideration when designing the most economically cost-effective tower.

The first operational prototype [Haaf *et al.* 1983] was built in Manzanares, Spain, in 1982 and the tower was constructed with thin iron sheets. The tower had operated for approximately eight years, but unfortunately, the tower had collapsed and was decommissioned in 1989 [Mills 2004] because the tower's guy-wires were not protected against corrosion and had failed due to rust and storm winds. To circumvent this issue, a different approach to building a rigid tower has been suggested by authors [Putkaradze *et al.* 2013] who proposed constructing the tower out of stacked inflatable tori. The shape of the tower would be such that the deformation due to wind loading is spread uniformly along the tower. There are several advantages of making an inflatable tower. One would be the potential to reducing the overall costs to erect and maintain a tall tower. The tower can be deflated and re-inflated for repairs and for situations such as severe weather conditions. Damages to the tower can be avoided quite easily and will substantially lower the costs for repairs. The inflatable tori can be pressurized individually by using remote pumps. It is interesting to consider the dynamics of the inflatable tower and whether or not the tower can withstand fierce winds.

The main focus of the dissertation is to analyze the dynamics of the inflatable tower and to study the tower's stability. The motion of the tower can

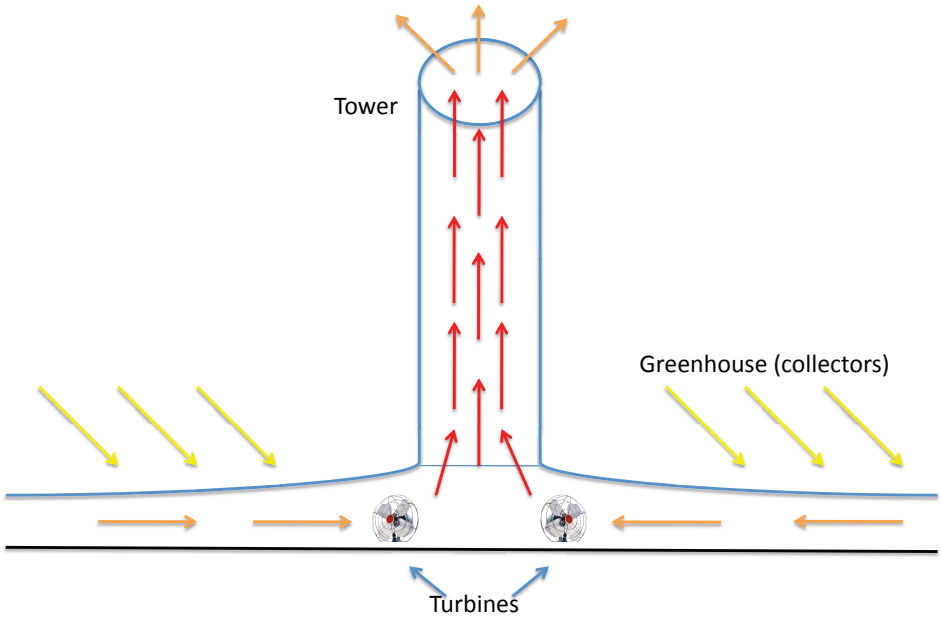

Figure 1.1: Schematic diagram of solar updraft tower with chimney.

be seen as a rigid body undergoing rotations, although it's not quite exactly a rigid body since the toroidal elements can be deformed from the compression of adjacent tori. The methods of geometric mechanics will be helpful to determine geometrically exact equations for the motion of the tower. Free rigid motion and principles from Lagrangian mechanics will be briefly stated before deriving the equations for the tower.

1.A Free rigid rotation

In free rigid rotation [Holm 2008], a body rotates about its centre of mass and the pairwise distances between all points in the body remain fixed. A system of coordinates in free rigid motion is stationary in a rotating orthonormal basis.

This rotating orthonormal basis is given by

$$\mathbf{e}_i(t) = \Lambda(t)\mathbf{E}_i(0) \ , \quad i = 1, 2, 3, \tag{1.1}$$

where $\Lambda(t)$ is an orthogonal 3×3 matrix, $\Lambda^{-1} = \Lambda^T$.

The unit vectors $\mathbf{E}_i(0), i = 1, 2, 3$ denote an orthonormal basis for fixed reference coordinates. Every point $\mathbf{r}(t)$ in rigid motion may be written in either coordinate basis as

$$\mathbf{r}(t) = r_0^j(t)\mathbf{E}_j(0), \tag{1.2}$$

$$= r^i\mathbf{e}_i(t), \tag{1.3}$$

where the components r^i satisfy $r^i = \delta^i_j r^j_0(0)$ for the choice that the two bases are initially aligned.

Using the orthogonality of $\Lambda(t)$, that is $\Lambda(t)\Lambda^T(t) = Id$, we may differentiate this equation with respect to time to obtain

$$\begin{aligned} 0 = \frac{d}{dt}\left(\Lambda(t)\Lambda^T(t)\right) &= \dot{\Lambda}(t)\Lambda^T(t) + \Lambda(t)\dot{\Lambda}^T(t) \\ &= \dot{\Lambda}(t)\Lambda^T(t) + \left(\dot{\Lambda}(t)\Lambda^T(t)\right)^T \\ &= \dot{\Lambda}(t)\Lambda^{-1}(t) + \left(\dot{\Lambda}(t)\Lambda^{-1}(t)\right)^T \\ &= \omega + \omega^T \end{aligned}$$

where $\omega := \dot{\Lambda}(t)\Lambda^{-1}(t)$. From the above computation, it follows that the matrix ω is skew-symmetric which allows one to introduce the corresponding angular velocity vector $\boldsymbol{\omega}(t) \in \mathbb{R}^3$. The components $\omega_k(t)$ of the angular

velocity vector, with $k = 1, 2, 3$, are given by

$$\omega_{ij}(t) = -\epsilon_{ijk}\omega_k(t) \ , \tag{1.4}$$

where ϵ_{ijk} is the anti-symmetric tensor.

Equation (1.4) defines the hat map, and one may write the matrix components of ω in terms of the components of $\boldsymbol{\omega}$ as

$$\omega = \begin{bmatrix} 0 & -\omega_3 & \omega_2 \\ \omega_3 & 0 & -\omega_1 \\ -\omega_2 & \omega_1 & 0 \end{bmatrix} \ . \tag{1.5}$$

The velocity in space of a point at $\mathbf{r}$ is found by

$$\dot{r}(t) = r^i \dot{e}_i(t) = r^i \dot{\Lambda}(t)\mathbf{e}_i(0) \tag{1.6}$$

$$= r^i \dot{\Lambda}(t)\Lambda^{-1}(t)\Lambda(t)\mathbf{e}_i(0) \tag{1.7}$$

$$= r^i \omega \mathbf{e}_i(t) \tag{1.8}$$

$$= \omega \mathbf{r}(t) \tag{1.9}$$

$$= \boldsymbol{\omega} \times \mathbf{r}(t) \ . \tag{1.10}$$

Thus, the velocity of free rigid motion of a point displaced by $\mathbf{r}$ from the centre of mass is a rotation in space of $\mathbf{r}$ about the time-dependent angular velocity vector $\boldsymbol{\omega}(t)$.

Remark (Notation): In (1.10), the notation $\omega \in \mathfrak{so}(3)$ is used for the anti-symmetric matrix corresponding to the vector $\boldsymbol{\omega} \in \mathbb{R}^3$. Throughout the rest of the dissertation, vectors in $\mathbb{R}^3$ will be denoted by bold symbols $\mathbf{v} \in \mathbb{R}^3$

and their corresponding antisymmetric matrix will be denoted by regular symbols $v \in \mathfrak{so}(3)$. They verify the relation $v = \widehat{\mathbf{v}}$, where the hat map $\mathbf{v} \in \mathbb{R}^3 \mapsto \widehat{\mathbf{v}} \in \mathfrak{so}(3)$ is the Lie algebra isomorphism defined by $\widehat{\mathbf{v}}\mathbf{x} = \mathbf{v} \times \mathbf{x}$, for all $\mathbf{x} \in \mathbb{R}^3$.

1.B The principle of stationary action

In Lagrangian mechanics, a mechanical system in a configuration space with generalised coordinates and velocities, $q^i, \dot{q}^i, i = 1, 2, \ldots, 3N$, is characterised by its Lagrangian defined as

$$L(q, \dot{q}) := K(q, \dot{q}) - U(q), \tag{1.11}$$

where $K(q, \dot{q})$ is the kinetic energy and $U(q)$ is the potential energy of the system. The motion of a Lagrangian system is determined by the principle of stationary action, formulated using the operation of variational derivative.

The variational derivative of a functional $S[q]$ is defined as its linearisation in an arbitrary direction δq in the configuration space. That is, $S[q]$ is defined as

$$\delta S[q] := \lim_{\varepsilon \to 0} \frac{S[q + \varepsilon \delta q] - S[q]}{\varepsilon} = \frac{d}{d\varepsilon}\Big|_{\varepsilon=0} S[q + \varepsilon \delta q] =: \left\langle \frac{\delta S}{\delta q}, \delta q \right\rangle, \tag{1.12}$$

where the pairing $\langle \cdot, \cdot \rangle$ is obtained in the process of linearisation.

The Euler-Lagrange equations,

$$[L]_{q^i} := \frac{d}{dt}\frac{\partial L}{\partial \dot{q}^i} - \frac{\partial L}{\partial q^i} = 0 \ , \tag{1.13}$$

follows from stationarity of the action integral, S, defined as the integral over a time interval $t \in (t_1, t_2)$,

$$S = \int_{t_1}^{t_2} L(q, \dot{q}) dt. \tag{1.14}$$

Then the principle of stationary action, also known as Hamilton's principle,

$$\delta S = 0 \tag{1.15}$$

implies $[L]_{q^i} = 0$, for variations δq^i that vanish at the endpoints of time.

To demonstrate the methods of geometric mechanics, which will be used later on more complex systems, let us apply the principle to the Lagrangian

$$L(\boldsymbol{\omega}) = \frac{1}{2}\mathbf{I}\boldsymbol{\omega} \cdot \boldsymbol{\omega}, \tag{1.16}$$

where $K(\boldsymbol{\omega}) = \frac{1}{2}\mathbf{I}\boldsymbol{\omega} \cdot \boldsymbol{\omega}$ is the kinetic energy of a rigid body and $\widehat{\boldsymbol{\omega}} := \Lambda^{-1}\dot{\Lambda} \in \mathfrak{so}(3)$ is the anti-symmetric matrix corresponding to the angular velocity vector $\boldsymbol{\omega}$. The variation $\delta\boldsymbol{\omega}$ induced by the variation $\delta\Lambda$ is computed as follows:

$$\begin{aligned}
\delta\widehat{\boldsymbol{\omega}} = \delta(\Lambda^{-1}\dot{\Lambda}) &= \delta(\Lambda^{-1})\dot{\Lambda} + \Lambda^{-1}\delta\dot{\Lambda} \\
&= -\Lambda^{-1}\delta\Lambda\Lambda^{-1}\dot{\Lambda} + \dot{\Sigma} + \omega\Sigma \\
&= \dot{\widehat{\boldsymbol{\Sigma}}} + \omega\Sigma - \Sigma\omega \\
&= \dot{\widehat{\boldsymbol{\Sigma}}} + \widehat{\boldsymbol{\omega} \times \boldsymbol{\Sigma}}
\end{aligned}$$

where $\Sigma := \Lambda^{-1}\delta\Lambda \in \mathfrak{so}(3)$ is an arbitrary curve satisfying $\Sigma(0) = \Sigma(T) = 0$.

The second line of the calculation uses the relation

$$\dot{\Sigma} = -\Lambda^{-1}\dot{\Lambda}\Lambda^{-1}\delta\Lambda + \Lambda^{-1}\delta\dot{\Lambda} = -\omega\Sigma + \Lambda^{-1}\delta\dot{\Lambda}.$$

The last line uses the commutator of two anti-symmetric matrices which corresponds to the cross product of their corresponding angular velocity vectors, i.e. $[\omega, \Sigma] := \omega\Sigma - \Sigma\omega = \widehat{\boldsymbol{\omega} \times \boldsymbol{\Sigma}}$. Thus we obtain

$$\delta\boldsymbol{\omega} = \dot{\boldsymbol{\Sigma}} - \boldsymbol{\Sigma} \times \boldsymbol{\omega}.$$

Using Hamilton's principle of stationary action gives

$$\delta \int_0^T L(\boldsymbol{\omega})dt = \int_0^T \frac{\delta L}{\delta \boldsymbol{\omega}} \cdot \delta\boldsymbol{\omega} dt = 0.$$

Integration by parts yields

$$\begin{aligned}
\int_0^T \frac{\delta L}{\delta \boldsymbol{\omega}} \cdot \delta\boldsymbol{\omega} \mathrm{d}t &= \int_0^T \frac{\delta L}{\delta \boldsymbol{\omega}} \cdot \left(\dot{\boldsymbol{\Sigma}} - \boldsymbol{\Sigma} \times \boldsymbol{\omega} \right) \mathrm{d}t \\
&= \int_0^T \left[-\frac{d}{dt}\left(\frac{\delta L}{\delta \boldsymbol{\omega}} \right) \cdot \boldsymbol{\Sigma} - \boldsymbol{\omega} \times \frac{\delta L}{\delta \boldsymbol{\omega}} \cdot \boldsymbol{\Sigma} \right] \mathrm{d}t + \frac{\delta L}{\delta \boldsymbol{\omega}} \cdot \boldsymbol{\Sigma} \Big|_0^T \\
&= -\int_0^T \left(\frac{d}{dt} + \boldsymbol{\omega} \times \right) \frac{\delta L}{\delta \boldsymbol{\omega}} \cdot \boldsymbol{\Sigma} \mathrm{d}t.
\end{aligned}$$

Since $\boldsymbol{\Sigma}$ is arbitrary, it follows that

$$\left(\frac{d}{dt} + \boldsymbol{\omega} \times \right) \frac{\delta L}{\delta \boldsymbol{\omega}} = 0 \ .$$

It is straightforward to see that

$$\frac{\delta L}{\delta \boldsymbol{\omega}} = \mathbf{I}\boldsymbol{\omega},$$

and thus the equations of motion are given by

$$\frac{d}{dt}\left(\mathbf{I}\boldsymbol{\omega}\right) = \mathbf{I}\boldsymbol{\omega} \times \boldsymbol{\omega}.$$

which is indeed the equation for rigid body motion.

Chapter 2

Methods of Geometric Mechanics

2.A Setup of the dynamical equations

Let us consider a flexible tower consisting of N toroidal elements with inner radius d_n and outer radius q_n, $n = 1, \ldots, N$, as shown in Fig. 2.1. In practice, these toroidal elements have different sizes so that the tower profile is optimized for both energy production and resistance to the wind. The latter requirement leads to the tower profile becoming narrower at the top following a certain law, as described in [Putkaradze *et al.* 2013]. In our theoretical considerations, we will use general d_n and q_n, however, all numerical simulations performed in this paper will use identical tori $q_n = q$ and $d_n = d$, so that the tower is cylindrical in its equilibrium form. The dynamics of each torus is described by giving the position $\mathbf{r}_n$ of its center, and the orientation of a moving basis $(\mathbf{e}_1^n, \mathbf{e}_2^n, \mathbf{e}_3^n)$ attached to the torus relative to a fixed spatial frame $(\mathbf{E}_1, \mathbf{E}_2, \mathbf{E}_3)$.

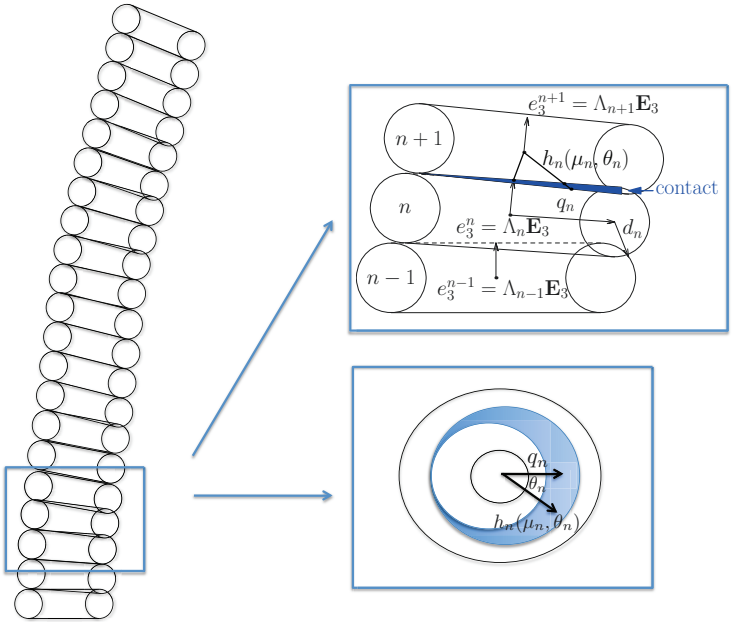

Figure 2.1: Setup of the system and explanation of variables used in the paper.

The moving basis is described by means of a rotation $\Lambda_n \in SO(3)$ such that

$$\mathbf{e}_i^n = \Lambda_n \mathbf{E}_i. \tag{2.1}$$

The general shape of each torus is assumed to not change, except for the compressed volume between the adjacent tori which we shall compute below. The pressures inside the tori is also assumed to equilibrate on far shorter scales than the typical time scales of the dynamics. The position and orientation is unified as a single element $(\Lambda, \mathbf{r})$ of the special Euclidean group $SE(3)$ with semi-direct product multiplication

$$(\Lambda, \mathbf{r}) \cdot (\Lambda', \mathbf{r}') = (\Lambda\Lambda', \Lambda\mathbf{r}' + \mathbf{r})\,. \tag{2.2}$$

The main premise of the theory is based on the symmetry invariance of the potential energy of deformations U_d.

Remark (On the symmetry invariance of tori interaction): Given the orientation and position of two adjacent tori $(\Lambda_n, \mathbf{r}_n)$ and $(\Lambda_{n+1}, \mathbf{r}_{n+1})$, the potential energy can only depend on the relative position and orientation, *i.e.* on the combination

$$(\Lambda_n, \mathbf{r}_n)^{-1} \cdot (\Lambda_{n+1}, \mathbf{r}_{n+1}) = (\Lambda_n^{-1}\Lambda_{n+1}, \Lambda_n^{-1}(\mathbf{r}_{n+1} - \mathbf{r}_n)) = (\mu_n, \mu_n \boldsymbol{\rho}_{n+1} - \boldsymbol{\rho}_n)\,, \tag{2.3}$$

where we have defined variables that are invariant with respect to *left* rotation

$$\mu_n := \Lambda_n^{-1}\Lambda_{n+1}\,, \quad \boldsymbol{\rho}_n := \Lambda_n^{-1}\mathbf{r}_n\,. \tag{2.4}$$

We thus have an expression of the form $U_d = \sum_{n=1}^{N-1} U_n(\mu_n, \boldsymbol{\rho}_n, \boldsymbol{\rho}_{n+1})$. We refer to [Ellis *et al.* 2010] for a detailed analysis of the $SE(3)$ invariance of dynamics in context of non locally interacting rods and its physical consequences.

This principle of invariance, stating that the potential energy U_d of the elastic deformation is invariant with respect to rotations and translations of the origin, must be verified for any physical model used in the quantitative description of the elastic energy. For example, one can obtain this energy through a computation of the volume overlap of two neighbouring undeformed tori. While this computation is straightforward, it is rather cumbersome and implicit for two tori in a generic position $\mathbf{r}_n$ and orientation Λ_n. Let us now provide one example of such a computation in the particular situation where the tori are in persistent contact. Let us choose the system of coordinates

for the n-th toroidal element so that θ is the angle sweeping along the large radius q_n, and α is the angle sweeping the small radius d_n. The deflection of the torus perpendicular to the plane swept by θ will be called $h_n(\mu_n, \theta)$ defining the shaded annulus-like area shown on Figure 2.1.

Remark (On contact between tori): If the position of the tori is unrestricted, for some (large) deformations $h_n(\mu_n, \theta)$ may degenerate to 0 for $|\theta| > \theta_m$ simply because one part of the torus loses contact with the neighbouring torus. The case that will be considered is where such loss of contact cannot occur. For example, the experimental realization of the tower, as explained in Chapter 5, consists of rubber inner tubes glued together along the large circle's perimeter. In that case, the tube is assumed to be in contact at all θ values, which leads to $h_n(\mu_n, \theta) \geq 0$ for $-\pi < \theta < \pi$. Technically, the persistence of contact means that the variables $\mathbf{r}_n$, μ_n satisfy a certain relationship and are no longer independent variables. However, the persistence of contact is determined by the details of tower construction; other situations such as *e.g* tori being attached with soft springs, will allow the loss of contact.

The potential energy of deformation of an individual torus is given by the work required to change the volume of a given element, i.e., $U_n = \int p_n \mathrm{d}V_n$. Assuming constant pressure, we have $U_n \simeq p_n \Delta V_n$. If the normal extent of the torus overlap is z, and the local curvature is d_n, then the width of the shaded area in Fig. 2.1 can be estimated as $\sqrt{2d_n z}$. We will approximate the integral $\oint h_n(\mu_n, \theta)^{3/2} \mathrm{d}\theta$ as a given fraction of its maximum value. The overlap volume

is estimated as

$$\Delta V_n = \oint \frac{4}{3}\sqrt{2d_n}h_n(\mu_n,\theta)^{3/2}q_n \mathrm{d}\theta \simeq C\sqrt{d_n}q_n h_{n,max}(\mu_n,\theta)^{3/2}\,, \tag{2.5}$$

where we have estimated the integral over $h_n(\mu_n,\theta)^{3/2}$ by its typical value $h^{3/2}_{n,max}(\theta)$ multiplied by the dimensionless constant that is less than 1. We have folded all dimensionless constants appearing in the integration into one single constant C, which will be dropped from further considerations. Thus, the total potential energy is

$$U_d = \sum_{n=1}^{N-1} p_n \Delta V_n = \sum_{n=1}^{N-1} p_n \oint \sqrt{d_n} h_n(\mu_n,\theta)^{3/2} q_n \mathrm{d}\theta \tag{2.6}$$

$$\simeq 2\pi \sum_{n=1}^{N-1} p_n q_n d_n^{1/2} h_{n,max}(\mu_n)^{3/2}\,. \tag{2.7}$$

Remark (Alternative energy expressions: symmetry invariance): The reader may notice that in our original setting U_d is a function of both μ_n and $\boldsymbol{\rho}_n, \boldsymbol{\rho}_{n+1}$, whereas in (2.7) the energy U_d depends only on μ_n. This happens because we assumed a perfect contact of tori which fixes the value of $\boldsymbol{\rho}_n$. In the description of other mechanical realizations of the tower, for example tori connected by springs or elastic material, U_d can depend on both μ_n and $\boldsymbol{\rho}_n$. Thus, our expression for the potential energy (2.7), while being rooted in physics, is necessarily simplistic. However, no matter how complex the potential energy U_n expression is considered, whether it is with or without persistent contact, it *must* satisfy the symmetry invariance, *i.e.* U_n reduce to be a function of μ_n, $\boldsymbol{\rho}_n$ and $\boldsymbol{\rho}_{n+1}$ only. Thus, we shall derive all the formulas in the most general case of a symmetry-invariant potential, and only use

expressions (2.7) for computations and comparison with experiments.

For future computations it is advantageous to simplify (2.7) for the case of two dimensional dynamics that we will use later. If $\mathbf{E}_3$ is the axis of symmetry of the torus, then the relative tilt, denoted as $\phi_n = \Delta\varphi_n$, is defined as

$$\cos\phi_n = \mathbf{e}_3^n \cdot \mathbf{e}_3^{n+1} = \Lambda_n \mathbf{E}_3 \cdot \Lambda_{n+1}\mathbf{E}_3 = \mathbf{E}_3 \cdot \Lambda_n^{-1}\Lambda_{n+1}\mathbf{E}_3 = \mathbf{E}_3 \cdot \mu_n \mathbf{E}_3, \quad (2.8)$$

giving the following expression for the potential energy:

$$U_d = 2\pi \sum_{n=1}^{N-1} p_n q_n d_n^{1/2} h_{n,max}(\mu_n)^{3/2} = 2\pi \sum_{n=1}^{N-1} p_n d_n^{1/2} q_n^{5/2} \sin|\Delta\varphi_n|^{3/2}\,, \quad (2.9)$$

where we used $h_{n,max}(\mu_n) = q_n \sin|\Delta\varphi_n|$. Note that a change of sign of $\Delta\varphi_n$ yields the same deformed volume and thus the same U_d, which leads to the absolute value sign in (2.9).

To consider the effect of gravity for 3D dynamics, the potential energy (2.9) is augmented by the gravity potential

$$U_g(\boldsymbol{\rho}, \boldsymbol{\kappa}) = \sum_{n=1}^{N} M_n \mathbf{r}_n \cdot \mathbf{g} = \sum_{n=1}^{N} M_n \boldsymbol{\rho}_n \cdot \Lambda_n^{-1}\mathbf{g} = \sum_{n=1}^{N} M_n \boldsymbol{\rho}_n \cdot \boldsymbol{\kappa}_n\,, \quad (2.10)$$

where M_n is the mass of n-th torus, $\boldsymbol{\kappa} := (\boldsymbol{\kappa}_1, ..., \boldsymbol{\kappa}_N)$, and we have defined the new variable

$$\boldsymbol{\kappa}_n := \Lambda_n^{-1}\mathbf{g} \in \mathbb{R}^3. \quad (2.11)$$

This variable verifies the additional dynamics

$$\dot{\boldsymbol{\kappa}}_n = -\omega_n \boldsymbol{\kappa}_n = -\boldsymbol{\omega}_n \times \boldsymbol{\kappa}_n, \quad (2.12)$$

where $\omega_n := \Lambda_n^{-1}\dot{\Lambda}_n \in \mathfrak{so}(3)$ and $\boldsymbol{\omega}_n \in \mathbb{R}^3$ is the angular velocity vector obtained from the antisymmetric matrix ω_n via the map $\mathbf{v} \in \mathbb{R}^3 \mapsto \widehat{\mathbf{v}} \in \mathfrak{so}(3)$. For simplicity, this potential energy contribution will be neglected in our numerical simulations. The kinetic energy is

$$K(\boldsymbol{\omega}, \boldsymbol{\gamma}) = \frac{1}{2}\sum_{n=1}^{N} \mathbf{I}_n \boldsymbol{\omega}_n \cdot \boldsymbol{\omega}_n + M_n |\boldsymbol{\gamma}_n|^2 \,, \quad \text{where} \quad \boldsymbol{\gamma}_n := \Lambda_n^{-1}\dot{r}_n \,, \tag{2.13}$$

and thus the Lagrangian of the system reads

$$\ell(\boldsymbol{\omega}, \boldsymbol{\gamma}, \boldsymbol{\rho}, \boldsymbol{\mu}, \boldsymbol{\kappa}) = \frac{1}{2}\sum_{n=1}^{N} \left(\mathbf{I}_n \boldsymbol{\omega}_n \cdot \boldsymbol{\omega}_n + M_n |\boldsymbol{\gamma}_n|^2\right) - U_d(\boldsymbol{\mu}, \boldsymbol{\rho}) - U_g(\boldsymbol{\rho}, \boldsymbol{\kappa}) \,, \tag{2.14}$$

where we used the notations $\boldsymbol{\omega} = (\boldsymbol{\omega}_1, ..., \boldsymbol{\omega}_N)$, $\boldsymbol{\gamma} = (\boldsymbol{\gamma}_1, ..., \boldsymbol{\gamma}_N)$.

It is important to note that the potential energy is proportional to the excessive pressure in each torus p_n. Similarly, if we denote the ambient atmospheric pressure as p_0, the density of air at each torus is proportional to the total pressure $p_0 + p_n$ assuming temperature is constant. Thus, for a given volume, we obtain that both the mass and moment of inertia of n-th torus are proportional to $p_n + p_0$, i.e., $M_n = (p_n + p_0)M_{0,n}$ and $\mathbf{I}_n = (p_n + p_0)\mathbf{I}_0$. We can thus rewrite the complete symmetry-reduced Lagrangian $\ell := \ell(\boldsymbol{\omega}, \boldsymbol{\gamma}, \boldsymbol{\rho}, \boldsymbol{\mu}, \boldsymbol{\kappa})$ as follows

$$\begin{aligned} \ell = \frac{1}{2}\sum_{n=1}^{N} &(p_n + p_0)\left(\mathbf{I}_0 \boldsymbol{\omega}_n \cdot \boldsymbol{\omega}_n + M_{0,n}|\boldsymbol{\gamma}_n|^2\right) \\ &- p_n U_{0,n}(\mu_n, \boldsymbol{\rho}_n, \boldsymbol{\rho}_{n+1}) - (p_n + p_0)\, M_{0,n}\boldsymbol{\rho}_n \cdot \boldsymbol{\kappa}_n \,. \end{aligned} \tag{2.15}$$

Here, we have defined a deformation function $U_{0,n}(\mu_n, \boldsymbol{\rho}_n, \boldsymbol{\rho}_{n+1})$ as the term multiplying the pressure in the relative deformation energy U_n, *i.e.*, $U_n = p_n U_{0,n}(\mu_n, \boldsymbol{\rho}_n, \boldsymbol{\rho}_{n+1})$. In what follows, we shall assume for simplicity that the

tori are identical, $q_n = q$ and $d_n = d$, leading to the universal energy function $U_0(\mu_n, \boldsymbol{\rho}_n, \boldsymbol{\rho}_{n+1})$; the formulas generalize in a rather straightforward way to more complex geometries. The quantities with the subscript 0 denote the variables independent of the pressure and depending only on the spatial dimension of each torus.

2.B Derivation of the equations of motion

The derivation is carried out using the Euler-Poincaré theory for the interacting elastic components. The Hamiltonian form of this framework was pioneered by Simo, Marsden, and Krisnaprasad [Simó *et al.* 1988], while the Lagrangian formulation of this theory including reduction by symmetries and discrete interactions was derived subsequently in [Holm & Putkaradze 2009], [Ellis *et al.* 2010], [Benoit *et al.* 2011]. The equations of motion are derived by using a symmetry reduced version of Hamilton's principle

$$\delta \int_0^T L(q, \dot{q}) \mathrm{d}t = 0, \tag{2.16}$$

where the Lagrangian, $L : TQ \to \mathbb{R}$, is defined on the tangent bundle TQ of the configuration space Q. In the present case, we have $\Lambda_k \in SO(3)$ and $\mathbf{r}_k \in \mathbb{R}^3$, forming an element $(\Lambda_k, \mathbf{r}_k) \in SE(3)$, for $k = 1, \ldots, N$. The configuration space is $Q = SE(3)^N \ni (\boldsymbol{\Lambda}, \mathbf{r})$, where $\boldsymbol{\Lambda} := (\Lambda_1, \ldots, \Lambda_N)$ and $\mathbf{r} := (\mathbf{r}_1, \ldots, \mathbf{r}_N)$. Hamilton's principle thus reads

$$\delta \int_0^T L(\boldsymbol{\Lambda}, \mathbf{r}, \dot{\boldsymbol{\Lambda}}, \dot{\boldsymbol{r}}) dt = 0, \tag{2.17}$$

for all variations $\boldsymbol{\Lambda}, \mathbf{r}$ such that $\delta\boldsymbol{\Lambda}(0) = \delta\boldsymbol{\Lambda}(T) = 0, \delta\mathbf{r}(0) = \delta\mathbf{r}(T) = 0$.

The Lagrangian L can be written in terms of the body variables

$$\begin{aligned}
&\omega_k = \Lambda_k^{-1}\dot{\Lambda}_k \in \mathfrak{so}(3), \qquad && \boldsymbol{\gamma}_k = \Lambda_k^{-1}\dot{\boldsymbol{r}}_k \in \mathbb{R}^3,\ k = 1, ..., N \\
&\boldsymbol{\rho}_k = \Lambda_k^{-1}\mathbf{r}_k \in \mathbb{R}^3, && \boldsymbol{\kappa}_k = \Lambda_k^{-1}\mathbf{g} \in \mathbb{R}^3,\ \ k = 1, ..., N \\
&\mu_k = \Lambda_k^{-1}\Lambda_{k+1} \in SO(3), && \qquad\qquad k = 1, ..., N-1,
\end{aligned} \tag{2.18}$$

thus we can write $L(\boldsymbol{\Lambda}, \mathbf{r}, \dot{\boldsymbol{\Lambda}}, \dot{\boldsymbol{r}}) = \ell(\boldsymbol{\omega}, \boldsymbol{\gamma}, \boldsymbol{\rho}, \boldsymbol{\mu}, \boldsymbol{\kappa})$, where

$$\begin{aligned}
(\boldsymbol{\omega}, \boldsymbol{\gamma}, \boldsymbol{\rho}, \boldsymbol{\mu}, \boldsymbol{\kappa}) : &= (\omega_1, ..., \omega_N, \boldsymbol{\gamma}_1, ..., \boldsymbol{\gamma}_N, \boldsymbol{\rho}_1, ..., \boldsymbol{\rho}_N, \mu_1, ..., \mu_{N-1}, \boldsymbol{\kappa}_1, ..., \boldsymbol{\kappa}_N) \\
&\in (\mathfrak{se}(3) \times \mathbb{R}^3)^N \times SO(3)^{N-1} \times (\mathbb{R}^3)^N
\end{aligned} \tag{2.19}$$

We compute the variations in (2.18) induced from the free variations $\delta\Lambda_k$ and $\delta\mathbf{r}_k$ of the variables Λ_k and $\mathbf{r}_k$ as follows:

$$\begin{aligned}
\delta\widehat{\boldsymbol{\omega}}_k = \delta(\Lambda_k^{-1}\dot{\Lambda}_k) &= \delta(\Lambda_k^{-1})\dot{\Lambda}_k + \Lambda_k^{-1}\delta\dot{\Lambda}_k \\
&= -\Lambda_k^{-1}\delta\Lambda_k\Lambda_k^{-1}\dot{\Lambda}_k + \dot{\Sigma}_k + \omega_k\Sigma_k \\
&= \dot{\widehat{\boldsymbol{\Sigma}}}_k + \omega_k\Sigma_k - \Sigma_k\omega_k \\
&= \dot{\widehat{\boldsymbol{\Sigma}}}_k + \widehat{\boldsymbol{\omega}_k \times \boldsymbol{\Sigma}_k} \\
\delta\boldsymbol{\gamma}_k = \delta(\Lambda_k^{-1}\dot{\boldsymbol{r}}_k) &= \delta(\Lambda_k^{-1})\dot{\boldsymbol{r}}_k + \Lambda_k^{-1}\delta\dot{\boldsymbol{r}}_k \\
&= -\Lambda_k^{-1}\delta\Lambda_k\Lambda_k^{-1}\dot{\boldsymbol{r}}_k + \dot{\boldsymbol{\Psi}}_k + \omega_k\boldsymbol{\Psi}_k \\
&= \dot{\boldsymbol{\Psi}}_k + \omega_k\boldsymbol{\Psi}_k - \Sigma_k\boldsymbol{\gamma}_k \\
&= \dot{\boldsymbol{\Psi}}_k + \boldsymbol{\omega}_k \times \boldsymbol{\Psi}_k - \boldsymbol{\Sigma}_k \times \boldsymbol{\gamma}_k
\end{aligned}$$

$$
\begin{aligned}
\delta\boldsymbol{\rho}_k = \delta(\Lambda_k^{-1}\mathbf{r}_k) &= \delta(\Lambda_k^{-1})\mathbf{r}_k + \Lambda_k^{-1}\delta\mathbf{r}_k \\
&= -\Lambda_k^{-1}\delta\Lambda_k\Lambda_k^{-1}\mathbf{r}_k + \boldsymbol{\Psi}_k \\
&= \boldsymbol{\Psi}_k - \Sigma_k\boldsymbol{\rho}_k \\
&= \boldsymbol{\Psi}_k - \boldsymbol{\Sigma}_k \times \boldsymbol{\rho}_k \\
\delta\mu_k = \delta(\Lambda_k^{-1}\Lambda_{k+1}) &= \delta(\Lambda_k^{-1})\Lambda_{k+1} + \Lambda_k^{-1}\delta\Lambda_{k+1} \\
&= -\Lambda_k^{-1}\delta\Lambda_k\Lambda_k^{-1}\Lambda_{k+1} + \Lambda_k^{-1}\Lambda_{k+1}\Lambda_{k+1}^{-1}\delta\Lambda_{k+1} \\
&= \mu_k\Sigma_{k+1} - \Sigma_k\mu_k \\
\delta\boldsymbol{\kappa}_k = \delta(\Lambda_k^{-1}\mathbf{g}) &= \delta(\Lambda_k^{-1})\mathbf{g} \\
&= -\Lambda_k^{-1}\delta\Lambda_k\Lambda_k^{-1}\mathbf{g} \\
&= -\Sigma_k\boldsymbol{\kappa}_k \\
&= -\boldsymbol{\Sigma}_k \times \boldsymbol{\kappa}_k
\end{aligned}
$$

where

$$
\Sigma_k := \Lambda_k^{-1}\delta\Lambda_k \in \mathfrak{so}(3), \quad \boldsymbol{\Psi}_k := \Lambda_k^{-1}\delta\mathbf{r}_k \in \mathbb{R}^3 \tag{2.20}
$$

are arbitrary curves satisfying $\Sigma_k(0) = \Sigma_k(T) = 0$, $\boldsymbol{\Psi}_k(0) = \boldsymbol{\Psi}_k(T) = 0$. In the above computations, we have used the formulas that are derived by taking the time derivatives of the variables Σ_k and $\boldsymbol{\Psi}_k$,

$$
\begin{aligned}
\dot{\Sigma}_k &= -\Lambda_k^{-1}\dot{\Lambda}_k\Lambda_k^{-1}\delta\Lambda_k + \Lambda_k^{-1}\delta\dot{\Lambda}_k = -\omega_k\Sigma_k + \Lambda_k^{-1}\delta\dot{\Lambda}_k \ , \\
\dot{\boldsymbol{\Psi}}_k &= -\Lambda_k^{-1}\dot{\Lambda}_k\Lambda_k^{-1}\mathbf{r}_k + \Lambda_k^{-1}\delta\dot{r}_k = -\omega_k\boldsymbol{\Psi}_k + \Lambda_k^{-1}\delta\dot{r}_k \ .
\end{aligned}
$$

In summary, we obtain the variations

$$\begin{cases} \delta\boldsymbol{\omega}_k = \dot{\boldsymbol{\Sigma}}_k - \boldsymbol{\Sigma}_k \times \boldsymbol{\omega}_k \\ \delta\boldsymbol{\gamma}_k = \dot{\boldsymbol{\Psi}}_k + \boldsymbol{\omega}_k \times \boldsymbol{\Psi}_k - \boldsymbol{\Sigma}_k \times \boldsymbol{\gamma}_k \\ \delta\boldsymbol{\rho}_k = \boldsymbol{\Psi}_k - \boldsymbol{\Sigma}_k \times \boldsymbol{\rho}_k \\ \delta\mu_k = \mu_k\Sigma_{k+1} - \Sigma_k\mu_k \\ \delta\boldsymbol{\kappa}_k = -\boldsymbol{\Sigma}_k \times \boldsymbol{\kappa}_k, \end{cases} \tag{2.21}$$

Thus the Euler-Poincaré principle then reads

$$\begin{aligned} &\delta \int_0^T \ell(\boldsymbol{\omega}, \boldsymbol{\gamma}, \boldsymbol{\rho}, \boldsymbol{\mu}, \boldsymbol{\kappa})\mathrm{d}t \\ &= \int_0^T \left(\sum_{k=1}^{N} \frac{\delta\ell}{\delta\boldsymbol{\omega}_k} \cdot \delta\boldsymbol{\omega}_k + \frac{\delta\ell}{\delta\boldsymbol{\gamma}_k} \cdot \delta\boldsymbol{\gamma}_k + \frac{\delta\ell}{\delta\boldsymbol{\rho}_k} \cdot \delta\boldsymbol{\rho}_k + \frac{\delta\ell}{\delta\boldsymbol{\kappa}_k} \cdot \delta\boldsymbol{\kappa}_k + \sum_{k=1}^{N-1} \left\langle \frac{\delta\ell}{\delta\mu_k}, \delta\mu_k \right\rangle \right) \mathrm{d}t \\ &= 0 \ , \end{aligned}$$

with variations given by (2.21). This approach is rigorously justified by the process of Lagrangian reduction by symmetry and the details of the process can be found in [Chi *et al.* 2014]. Using integration by parts, we obtain

$$\begin{aligned} \int_0^T \frac{\delta\ell}{\delta\boldsymbol{\omega}_k} \cdot \delta\boldsymbol{\omega}_k \mathrm{d}t &= \int_0^T \frac{\delta\ell}{\delta\boldsymbol{\omega}_k} \cdot \left(\dot{\boldsymbol{\Sigma}}_k - \boldsymbol{\Sigma}_k \times \boldsymbol{\omega}_k \right) \mathrm{d}t \\ &= \int_0^T \left[-\frac{d}{dt} \left(\frac{\delta\ell}{\delta\boldsymbol{\omega}_k} \right) \cdot \boldsymbol{\Sigma}_k - \boldsymbol{\omega}_k \times \frac{\delta\ell}{\delta\boldsymbol{\omega}_k} \cdot \boldsymbol{\Sigma}_{\boldsymbol{k}} \right] \mathrm{d}t + \frac{\delta\ell}{\delta\boldsymbol{\omega}_k} \cdot \boldsymbol{\Sigma}_k \Big|_0^T \\ &= -\int_0^T \left(\frac{d}{dt} + \boldsymbol{\omega}_k \times \right) \frac{\delta\ell}{\delta\boldsymbol{\omega}_k} \cdot \boldsymbol{\Sigma}_k \mathrm{d}t \end{aligned}$$

$$
\begin{aligned}
\int_0^T \frac{\delta \ell}{\delta \boldsymbol{\gamma}_k} \cdot \delta \boldsymbol{\gamma}_k \mathrm{d}t &= \int_0^T \frac{\delta \ell}{\delta \boldsymbol{\gamma}_k} \cdot \left(\dot{\boldsymbol{\Psi}}_k + \boldsymbol{\omega}_k \times \boldsymbol{\Psi}_k - \boldsymbol{\Sigma}_k \times \boldsymbol{\gamma}_k \right) \mathrm{d}t \\
&= \int_0^T \left[-\frac{d}{dt} \left(\frac{\delta \ell}{\delta \boldsymbol{\gamma}_k} \right) \boldsymbol{\Psi}_k - \frac{\delta \ell}{\delta \boldsymbol{\gamma}_k} \cdot \boldsymbol{\Psi}_k \times \boldsymbol{\omega}_k - \boldsymbol{\gamma}_k \times \frac{\delta \ell}{\delta \boldsymbol{\gamma}_k} \cdot \boldsymbol{\Sigma}_k \right] \mathrm{d}t \\
&\quad + \frac{\delta \ell}{\delta \boldsymbol{\gamma}_k} \cdot \boldsymbol{\Psi}_k \Big|_0^T \\
&= -\int_0^T \left[\left(\frac{d}{dt} + \boldsymbol{\omega}_k \times \right) \frac{\delta \ell}{\delta \boldsymbol{\gamma}_k} \cdot \boldsymbol{\Psi}_k + \boldsymbol{\gamma}_k \times \frac{\delta \ell}{\delta \boldsymbol{\gamma}_k} \cdot \boldsymbol{\Sigma}_k \right] \mathrm{d}t \\
\int_0^T \frac{\delta \ell}{\delta \boldsymbol{\rho}_k} \cdot \delta \boldsymbol{\rho}_k \mathrm{d}t &= \int_0^T \frac{\delta \ell}{\delta \boldsymbol{\rho}_k} \cdot \left(\boldsymbol{\Psi}_k - \boldsymbol{\Sigma}_k \times \boldsymbol{\rho}_k \right) \mathrm{d}t \\
&= \int_0^T \left[\frac{\delta \ell}{\delta \boldsymbol{\rho}_k} \cdot \boldsymbol{\Psi}_k - \boldsymbol{\rho}_k \times \frac{\delta \ell}{\delta \boldsymbol{\rho}_k} \cdot \boldsymbol{\Sigma}_k \right] \mathrm{d}t \\
\int_0^T \frac{\delta \ell}{\delta \boldsymbol{\kappa}_k} \cdot \delta \boldsymbol{\kappa}_k \mathrm{d}t &= \int_0^T -\frac{\delta \ell}{\delta \boldsymbol{\kappa}_k} \cdot \boldsymbol{\Sigma}_k \times \boldsymbol{\kappa}_k \mathrm{d}t \\
&= -\int_0^T \boldsymbol{\kappa}_k \times \frac{\delta \ell}{\delta \boldsymbol{\kappa}_k} \cdot \boldsymbol{\Sigma}_k \mathrm{d}t \\
\sum_{k=1}^{N-1} \left\langle \frac{\delta \ell}{\delta \mu_k}, \delta \mu_k \right\rangle &= \sum_{k=1}^{N-1} \left\langle \frac{\delta \ell}{\delta \mu_k}, \mu_k \Sigma_{k+1} - \Sigma_k \mu_k \right\rangle \\
&= \sum_{k=1}^{N-1} \left\langle \frac{\delta \ell}{\delta \mu_k}, \mu_k \Sigma_{k+1} \right\rangle - \sum_{k=1}^{N-1} \left\langle \frac{\delta \ell}{\delta \mu_k}, \Sigma_k \mu_k \right\rangle \\
&= \sum_{k=1}^{N-1} \left\langle \mu_k^T \frac{\delta \ell}{\delta \mu_k}, \Sigma_{k+1} \right\rangle - \sum_{k=1}^{N-1} \left\langle \frac{\delta \ell}{\delta \mu_k} \mu_k^T, \Sigma_k \right\rangle \\
&= \sum_{k=2}^{N} \left\langle \mu_{k-1}^T \frac{\delta \ell}{\delta \mu_{k-1}}, \Sigma_k \right\rangle - \sum_{k=1}^{N-1} \left\langle \frac{\delta \ell}{\delta \mu_k} \mu_k^T, \Sigma_k \right\rangle \\
&= -\left\langle \frac{\delta \ell}{\delta \mu_1} \mu_1^T, \Sigma_1 \right\rangle + \sum_{k=2}^{N-1} \left\langle \mu_{k-1}^T \frac{\delta \ell}{\delta \mu_{k-1}} - \frac{\delta \ell}{\delta \mu_k} \mu_k^T, \Sigma_k \right\rangle \\
&\quad + \left\langle \mu_{N-1}^T \frac{\delta \ell}{\delta \mu_{N-1}}, \Sigma_N \right\rangle \\
&= \left\langle \mu_1 \frac{\delta \ell}{\delta \mu_1}^T - \frac{\delta \ell}{\delta \mu_1} \mu_1^T, \Sigma_1 \right\rangle \\
&\quad + \sum_{k=2}^{N-1} \left\langle \mu_{k-1}^T \frac{\delta \ell}{\delta \mu_{k-1}} - \mu_{k-1} \frac{\delta \ell}{\delta \mu_{k-1}}^T + \mu_k \frac{\delta \ell}{\delta \mu_k}^T - \frac{\delta \ell}{\delta \mu_k} \mu_k^T, \Sigma_k \right\rangle \\
&\quad + \left\langle \mu_{N-1}^T \frac{\delta \ell}{\delta \mu_{N-1}} - \frac{\delta \ell}{\delta \mu_{N-1}}^T \mu_{N-1}, \Sigma_N \right\rangle =: \sum_{k=1}^{N} \mathbf{Z}_k \cdot \boldsymbol{\Sigma}_k
\end{aligned}
$$

Here, $k = 1, 2, ..., N$ is the index of the tori and we defined the vector

$$\mathbf{Z}_k := \left(\mu_{k-1}^T \frac{\delta \ell}{\delta \mu_{k-1}} - \frac{\delta \ell}{\delta \mu_{k-1}}^T \mu_{k-1}\right)^\vee + \left(\mu_k \frac{\delta \ell}{\delta \mu_k}^T - \frac{\delta \ell}{\delta \mu_k} \mu_k^T\right)^\vee, \quad k = 1, 2, ..., N, \tag{2.22}$$

with the convention that when $k = 0$ or $k = N$, then $\mu_k = 0$. In that formula, $A \in \mathfrak{so}(3) \to A^\vee \in \mathbb{R}^3$ denotes the inverse of the hat map $\mathbf{v} \in \mathbb{R}^3 \mapsto \widehat{\mathbf{v}} \in \mathfrak{so}(3)$.

By taking terms proportional to $\mathbf{\Sigma}_k$ (giving the equation for angular momentum) and $\mathbf{\Psi}_k$ (defining the linear momentum equation), the equations of motion are given by

$$\begin{cases} \left(\frac{d}{dt} + \boldsymbol{\omega}_k \times\right) \frac{\delta \ell}{\delta \boldsymbol{\omega}_k} + \boldsymbol{\gamma}_k \times \frac{\delta \ell}{\delta \boldsymbol{\gamma}_k} + \boldsymbol{\rho}_k \times \frac{\delta \ell}{\delta \boldsymbol{\rho}_k} + \boldsymbol{\kappa}_k \times \frac{\delta \ell}{\delta \boldsymbol{\kappa}_k} = \mathbf{Z}_k \\ \left(\frac{d}{dt} + \boldsymbol{\omega}_k \times\right) \frac{\delta \ell}{\delta \boldsymbol{\gamma}_k} - \frac{\delta \ell}{\delta \boldsymbol{\rho}_k} = 0 \end{cases} . \tag{2.23}$$

Remark (Functional derivatives): The functional derivatives $\frac{\delta \ell}{\delta \boldsymbol{\omega}_k}, \frac{\delta \ell}{\delta \boldsymbol{\gamma}_k}, \frac{\delta \ell}{\delta \boldsymbol{\rho}_k} \in \mathbb{R}^3$ are computed with the usual inner product on $\mathbb{R}^3$, i.e., $\mathbf{x} \cdot \mathbf{y} = x_1 y_1 + x_2 y_2 + x_3 y_3 = \frac{1}{2} \operatorname{Tr}(\widehat{\mathbf{x}}^\top \widehat{\mathbf{y}})$, and the functional derivatives $\frac{\delta \ell}{\delta \mu_k} \in T_{\mu_k}^* SO(3)$ are computed with the left and right invariant pairing $\langle A, B \rangle := \frac{1}{2} \operatorname{Tr}(A^\top B)$.

Including wind torque. The torque due to the wind on the element n is given from the torques due to wind acting on all the elements above n. For simplicity we can assume that the velocity of the wind is the same for all elevations, and the module of the force of the wind on the n-th element is $C_D \rho S_n U_w^2$, with $S_n = \pi d_n^2 + q_n d_n$ being the area exposed to the wind in the fully inviscid approximation, ρ being density of air and C_D being the drag coefficient. This formula is adequate as a first order approximation of the force and will be used in our simulations. The drag force due to the wind

resistance is acting in the direction of the wind, *i.e.* the $\mathbf{E}_2$ direction. The other components of wind resistance, acting perpendicular to the wind when the n-th torus is inclined, cause tower compression but do not contribute to the total torque on the tower and thus will be ignored. The torque due to the wind is computed as follows. In the spatial (steady) frame, the wind force on the k-th torus is $\mathbf{F}_k^{\text{wind}} = C_D \rho S_k U_w^2 \mathbf{e}_2$. Here, U_w is the wind speed, and the wind is assumed to be always in $\mathbf{e}_2$ direction. The torque applied by this force, with respect of the center of the n-th torus ($n < k$) is $(\mathbf{r}_k - \mathbf{r}_n) \times \mathbf{F}_k$. So the total torque in the spatial frame due to the tori $n+1, n+2, ..., N$, with respect to the center of the n-th torus is

$$\mathbf{T}_{sp,n} = \sum_{k=n+1}^{N} (\mathbf{r}_k - \mathbf{r}_n) \times \mathbf{F}_k^{\text{wind}}. \tag{2.24}$$

To incorporate this torque into our framework, we convert this expression in the convective frame by multiplying by Λ_n^{-1} to get

$$\mathbf{T}_n = \Lambda_n^{-1} \sum_{k=n+1}^{N} (\mathbf{r}_k - \mathbf{r}_n) \times \mathbf{F}_k^{\text{wind}} = C_D \rho S_k U_w^2 \sum_{k=n+1}^{N} \Lambda_n^{-1}(\mathbf{r}_k - \mathbf{r}_n) \times \Lambda_n^{-1} \mathbf{E}_2 \,. \tag{2.25}$$

Equation (2.25) is appropriate for large deformations of the tower; however, it is rather awkward to use in invariant coordinates because of the term $\Lambda_n^{-1}\mathbf{r}_k$ which is expressed as a product

$$\Lambda_n^{-1}\mathbf{r}_k = \mu_n \mu_{n+1} \ldots \mu_{k-1} \boldsymbol{\rho}_k \,. \tag{2.26}$$

We shall show below that (2.25) allows simplification for the case of two-dimensional motion.

The equations in presence of the wind torque $\mathbf{T}_n$ are derived via the Lagrange-d'Alembert principle

$$\delta \int_0^T \ell(\boldsymbol{\omega}, \boldsymbol{\gamma}, \boldsymbol{\rho}, \boldsymbol{\mu}, \boldsymbol{\kappa}) \mathrm{d}t + \int_0^T \mathbf{T} \cdot \boldsymbol{\Sigma} \, \mathrm{d}t = 0 \,, \text{ with respect to the variations (2.21)} \,. \tag{2.27}$$

In this case, the first equation of (2.23) becomes

$$\left(\frac{d}{dt} + \boldsymbol{\omega}_k \times \right) \frac{\delta \ell}{\delta \boldsymbol{\omega}_k} + \boldsymbol{\gamma}_k \times \frac{\delta \ell}{\delta \boldsymbol{\gamma}_k} + \boldsymbol{\rho}_k \times \frac{\delta \ell}{\delta \boldsymbol{\rho}_k} + \boldsymbol{\kappa}_k \times \frac{\delta \ell}{\delta \boldsymbol{\kappa}_k} = \mathbf{Z}_k + \mathbf{T}_k, \tag{2.28}$$

while the second equation is unchanged.

Chapter 3

Two-Dimensional Dynamics

To make further progress, let us apply the theory derived in the previous section, which is valid for arbitrary Lagrangians, to the particular case of the tower comprised from inflatable tori. In that case, we shall assume that the main deformation of the tori comes from bending the tower and not mutual compression. The bending is assumed to be always in the plane which is collinear with the wind direction. We shall also make the non-essential assumption that the mass of the material of the tori is much less than the excessive mass coming from over-pressurizing the torus itself. This leads to some simplifications of the equations, although more general cases can be considered easily.

All dynamics is assumed to occur in $(\mathbf{E}_1, \mathbf{E}_2)$ plane with $\mathbf{E}_1$ being the undisturbed (spatial) vertical axis of the tower. In this framework, denoting the tilt of the axis for k-th torus from the vertical axis as φ_k, we have

$$\Lambda_k = \exp(\varphi_k \mathbf{E}_3) = \begin{bmatrix} \cos\varphi_k & -\sin\varphi_k & 0 \\ \sin\varphi_k & \cos\varphi_k & 0 \\ 0 & 0 & 1 \end{bmatrix}, \tag{3.1}$$

so $\mu_k = \exp((\varphi_{k+1} - \varphi_k)\mathbf{E}_3) = \exp(\Delta\varphi_k \mathbf{E}_3)$ and $\boldsymbol{\omega}_k = \dot{\varphi}_k \mathbf{E}_3$. Note that in this section, $\mathbf{E}_3$ is orthogonal to the plane of motion, unlike the three-dimensional discussion above where $\mathbf{E}_3$ denoted the vertical axis. The position of the center of the n-th torus is given by

$$\mathbf{r}_n = \sum_{k=1}^{n-1} 2d_k \left(\cos\varphi_k, \sin\varphi_k\right) + d_n \left(\cos\varphi_n, \sin\varphi_n\right). \tag{3.2}$$

Then

$$\dot{\boldsymbol{r}}_n = \sum_{k=1}^{n-1} 2d_k \left(-\sin\varphi_k, \cos\varphi_k\right) \dot{\varphi_k} + d_n \left(-\sin\varphi_n, \cos\varphi_n\right) \dot{\varphi}_n \tag{3.3}$$

Assuming small deviations from equilibrium, *i.e.*, $|\varphi_k| << 1$ gives

$$\dot{\boldsymbol{r}}_n = \left(\sum_{k=1}^{n-1} 2d_k \dot{\varphi}_k + d_n \dot{\varphi}_n \right) \mathbf{E}_2. \tag{3.4}$$

Thus, denoting $\boldsymbol{\varphi} = (\varphi_1, ..., \varphi_N)^T$, the Lagrangian is given by

$$L(\boldsymbol{\varphi}, \dot{\boldsymbol{\varphi}}) = \sum_{n=1}^{N} \frac{1}{2} I_n \dot{\varphi}_n^2 + \sum_{n=1}^{N} M_n \left(\sum_{k=1}^{n-1} 2d_k \dot{\varphi}_k + d_n \dot{\varphi}_n \right)^2 - \sum_{n=1}^{N-1} p_n U_0(\Delta\varphi_n), \tag{3.5}$$

where $I_n = (p_0 + p_n) I_0$, $M_n = (p_n + p_0) M_{0,n}$ and we have assumed that due to the identical nature of the tori, the dependence of the potential energy on relative deformation is exactly the same for each torus and is given by the two-dimensional analogue of (2.9), i.e., $U_0(\Delta\varphi_n) = 2\pi q_n \sqrt{d_n h_n (\Delta\varphi_n)^3}$. We shall undertake a detailed calculation of the kinetic energy term later. For now, we simply mention that (3.5) can be written in terms of a symmetric

$N \times N$ matrix $\mathbb{S}$ as

$$L(\boldsymbol{\varphi}, \dot{\boldsymbol{\varphi}}) = \frac{1}{2} \sum_{k,l=1}^{N} \mathbb{S}_{kl} \dot{\varphi}_k \dot{\varphi}_l - \sum_{n=1}^{N-1} p_n U_0(\Delta\varphi_n)\,, \quad \mathbb{S}_{kl} = \mathbb{S}_{lk}\,, \tag{3.6}$$

since every quadratic form in $\dot{\boldsymbol{\varphi}}$ can be written in terms of an appropriate symmetric matrix.

Applying Hamilton's principle of stationary action yields the equations of motion

$$\left(\mathbb{S}\ddot{\boldsymbol{\varphi}}\right)_n + p_{n-1} U_0'\left(\Delta\varphi_{n-1}\right) - p_n U_0'\left(\Delta\varphi_n\right) = 0, \;\; n = 1, ..., N, \tag{3.7}$$

with the appropriate modifications for $n = 1$ (bottom torus) and $n = N$ (top torus).

In the presence of the wind, the external torques added to the right hand side of (3.7) are computed by simplifying the expression (2.25) as follows. Assume that the deformations from equilibrium are small and so $\mathbf{r}_k \simeq \mathbf{E}_3 z_k$, with z_k being a scalar height variable. In that approximation, using (2.25) we also get $\Lambda_n^{-1}\mathbf{r}_k \simeq \mathbf{E}_3 z_k$. Since $\Lambda_n^{-1}\mathbf{e}_3 = \mathbf{E}_3$ and $\mathbf{E}_3 \times \mathbf{E}_2 = -\mathbf{E}_1$, we get the approximate, but easy to use, expression for the wind torque

$$\mathbf{T}_n = U_w^2 \sum_{k=n+1}^{N} S_k z_{k,n} \mathbf{E}_3 \times \mathbf{E}_2 = -\mathbf{E}_1 U_w^2 \sum_{k=n+1}^{N} S_k z_{k,n}. \tag{3.8}$$

Chapter 4

Numerical Simulations

We shall confine all numerical simulations to two-dimensional dynamics, where the motion is limited to $(\mathbf{E}_1, \mathbf{E}_2)$ plane and all the rotations are about $\mathbf{E}_3$ axis, as in Chapter 3. In this case $h_n = q_n \sin|\Delta\varphi_n|$. The parameters for simulations are as follows: all tori are assumed of equal size with $d_n = 1\text{m}$, $q_n = 3\text{m}$, temperature $T = 300\text{K}$ and overpressure $p_n = 10^5$ Pa $= 1\text{atm}$.

For further consideration, it is convenient to explicitly separate the dependence on the pressure p_n in each torus. We define $U_0 := U/p_n$, the scaled energy having dimensions of volume. Then the scaled energy for the n^{th} torus as well as corresponding derivatives are given by

$$\begin{cases} \dfrac{\partial U_0}{\partial h_n} = \dfrac{3}{2} K q_n \sqrt{r_n h_n}, \quad \dfrac{\partial^2 U_0}{\partial h_n^2} = \dfrac{3}{4} K q_n \sqrt{\dfrac{r_n}{h_n}}, \\ \\ \dfrac{\partial h_n}{\partial \Delta\varphi_n} = \dfrac{q_n^2 \sin^2(2|\Delta\varphi_n|)}{2h_n}, \dfrac{\partial^2 h_n}{\partial(\Delta\varphi_n)^2} = \dfrac{q_n^2 \cos(2|\Delta\varphi_n|)}{h_n} - \dfrac{q_n^4 \sin^2(2|\Delta\varphi_n|)}{4h_n^3} \end{cases} \tag{4.1}$$

Using chain rule, we obtain

$$U_0'(\Delta\varphi_n) = \frac{\partial U_0}{\partial h_n} \cdot \frac{\partial h_n}{\partial \Delta\varphi_n} = \frac{3}{4} K \sqrt{\frac{r_n}{h_n}} q_n^3 \sin(2|\Delta\varphi_n|). \tag{4.2}$$

Note that $h_n \sim |\Delta\phi_n|$, so we have $U_0'(\Delta\phi_n) \sim |\Delta\phi_n|^{\frac{1}{2}}$; thus the system is fully nonlinear. Since $U_0'(\Delta\phi_n) \sim |\Delta\phi_n|^{\frac{1}{2}}$, the straight configuration is 'super-linearly stable' since it has a faster growing restoring force than any linear function but may be nonlinearly unstable due to gravity if the tower is weakly inflated. Taking the second derivative yields

$$U_0''(\Delta\varphi_n) = \frac{\partial^2 U_0}{\partial h_n^2} \cdot \left(\frac{\partial h_n}{\partial \Delta\varphi_n}\right)^2 + \frac{\partial U_0}{\partial h_n} \cdot \frac{\partial^2 h_n}{\partial (|\Delta\varphi_n|)^2} \tag{4.3}$$

$$= \frac{3}{16} K \sqrt{\frac{r_n}{h_n}} q_n^3 \left(8\cos(2|\Delta\varphi_n|) - \frac{q_n^2 \sin^2(2|\Delta\varphi_n|)}{h_n^2}\right). \tag{4.4}$$

Note that $U_0'(\Delta\phi_n) \sim |\Delta\phi_n|^{-1/2}$ for small $\Delta\phi_n$ and for $\epsilon = 0$, thus U_0'' is unbounded at the origin. This leads to the absence of natural resonance frequencies.

We compute the dynamics given by (3.7) for a tower consisting of $N = 20$ identical tori. For the purpose of regularization and error control we use the following smoothing of the $h_n \sim |\Delta\phi|$

$$h_n \approx q_n \sqrt{\epsilon^2 + \sin^2(\Delta\varphi_n)}\,, \quad \epsilon \ll 1\,. \tag{4.5}$$

Using the approximation for h_n, we obtain

$$U_0''(\Delta\varphi_n) \approx \frac{3}{16} K \frac{r_n^{\frac{1}{2}} q_n^{\frac{5}{2}}}{(\epsilon^2 + \sin^2(\Delta\varphi_n))^{\frac{1}{4}}} \left(8\cos(2|\Delta\varphi_n|) - \frac{\sin^2(2|\Delta\varphi_n|)}{\epsilon^2 + \sin^2(\Delta\varphi_n)}\right), \tag{4.6}$$

and thus

$$U_0''(0) \approx \frac{3}{16} K \frac{r_n^{\frac{1}{2}} q_n^{\frac{5}{2}}}{\epsilon^{\frac{1}{2}}}. \tag{4.7}$$

For small oscillations, resonant frequencies will be proportional to typical values of $\sqrt{U_0''}$, and thus diverge as $\epsilon^{-1/4} \to 0$. Thus, regularization will not lead to appearance of resonance frequencies for physically relevant frequencies of wind forcing, which are typically small. For small ϵ, the system is stiff and thus an ODE solver an implicit scheme is used to perform the simulations since using Runge-Kutta's scheme was slow due to the stiffness. The solver will solve a set of non-linear (or linear) equations at each time step, for which will require the computation of the Jacobian of the system. The accuracy of the scheme is between 1-st order and 5-th order depending on the system (See Appendix A for numerical codes for MATLAB).

Snapshots of the tower shown in Fig. 4.1 depicts the motion bouncing back and forth about the straight configuration.

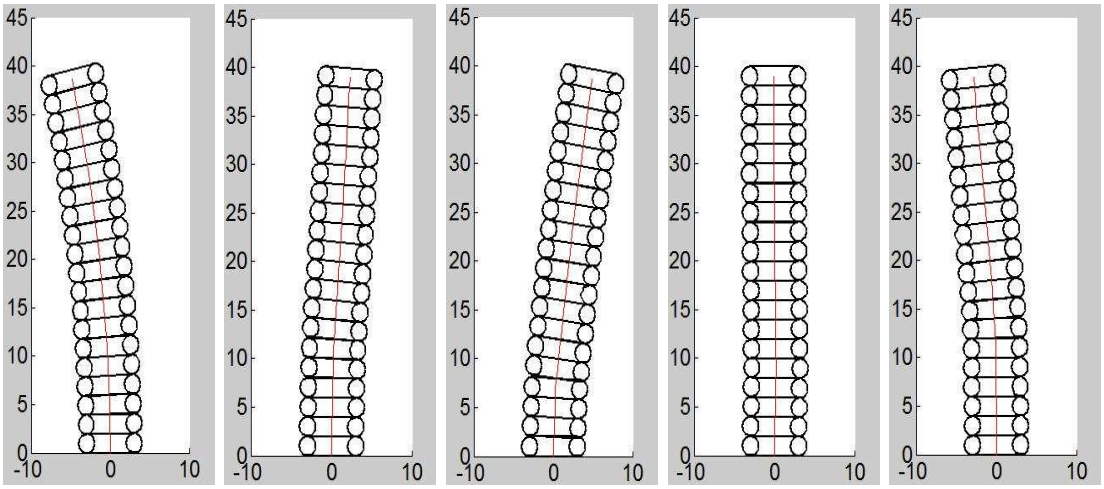

Figure 4.1: Snapshots of dynamics with 20 tori and parameters outlined as above. All sizes are in m.

Chapter 5

Experiments

An experimental prototype of a solar-chimney power plant was assembled and tested at the University of New Mexico on the roof of the Mechanical Engineering building to maximize exposure of apparatus to wind. The chimney proper (3 m tall) was constructed from a stack of forty motorcycle and scooter tire inner tubes Fig. 5.1 glued together following the proportional design scheme [Putkaradze *et al.* 2013]. The tower profile is a discrete approximation of the design scheme simply due to the limited available sizes of the inner tubes. The apparatus was designed to serve as a proof of principle for the inflatable tower concept, and to provide performance benchmarks for numerical modelling under realistic insolation and wind conditions, thus all the testing of wind resistance and dynamics was done outside. During the experiments, the chimney was exposed to a variety of weather conditions, including sustained winds exceeding 20 m/s. With higher values of overpressure, the tower demonstrated remarkable stability; unfortunately, deflections are very hard to measure in that case. Thus, in what follows, we concentrate on data collected at a modest overpressure of 0.17 atm which is far below the maximum rated

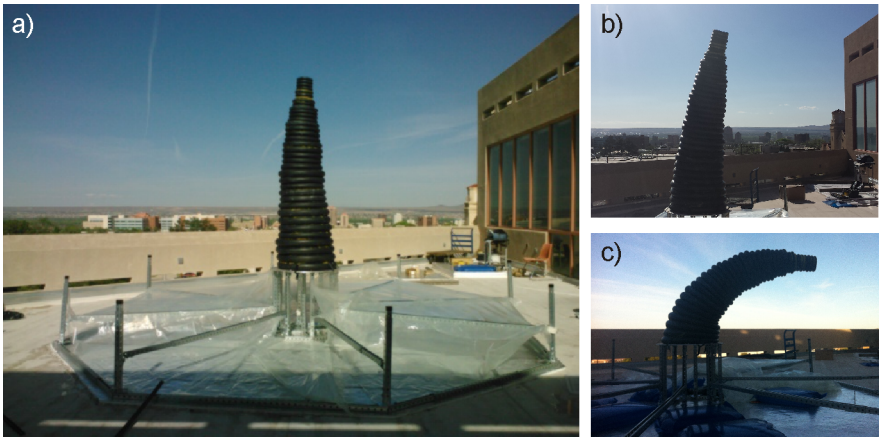

Figure 5.1: Photographs of UNM solar chimney prototype: a) wind speed 0.7 m/s from the south (left) and overall view, b) wind speed 2.2 m/s, c) wind speed 20.1 m/s. The overpressure in the tori is uniform at 0.17 atm.

pressure for the inner tubes in excess of 30 psi, or about 2 atm. This lower overpressure leads to a variety of interesting behaviours. Below, we focus on the static deflections only.

The overall viability of the inflatable-chimney design has been demonstrated, with even the small prototype producing measurable power and continuing operation after sunset because thermal storage elements under the greenhouse (water bladders) continued to release heat accumulated during the day. Moreover, the chimney survived some very strong winds, with gusts up to 27 m/s.

While the focus of this preliminary study was on the proof of concept, some measurements of the tower behaviour under wind loading were also acquired. First, deflection of the tower under wind loading was found to be consistent with the theoretical assumptions, with the tower deformation distributed smoothly along the stack of inflatable tori. The tower exposed to a wind speed of 20.1 m/s as shown in Fig. 5.1 does not recover from the large deformation due to gravity. In Table 5.1, the horizontal deflection of the top

of the tower with several measured wind speeds is presented.

Wind speed, m/s	0.8 ± 0.1	2.2 ± 0.2	3.1 ± 0.2	20.3 ± 0.3
Deflection, m	0.12 ± 0.02	0.35 ± 0.08	0.51 ± 0.10	2.02 ± 0.06

Table 5.1: Horizontal deflection of tower top vs. wind speed.

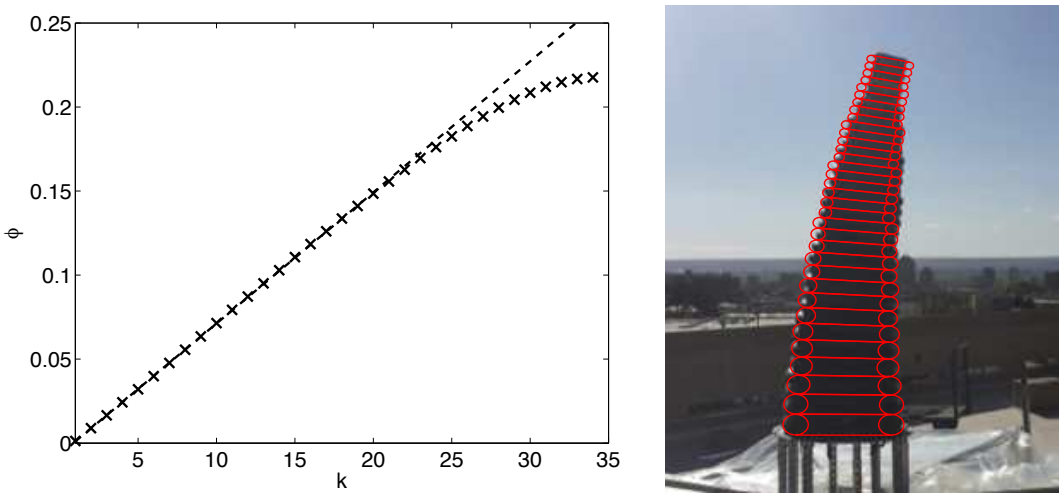

Figure 5.2: Left: steady deflection angles computed from (3.7). Notice almost linear dependence of ϕ_k on the height. Right: comparison of the shape given by a convergent steady state of (3.7) with experiments for 2.2 m/s wind speed.

A detailed comparison of the tower deflection with wind speed in the static configuration was performed corresponding to the medium wind speed – case b) in Fig. 5.1. To do so, a constant wind speed throughout the vertical direction was assumed, and a friction term proportional to $-\phi'(t)$ in the right-hand side of (3.7) was introduced, which made the system converge to a steady shape, independent of the friction coefficient. The result is shown in Fig. 5.2. All the sizes of the tori and overpressures were taken to be exactly equal to their experimental values. To match modelling with the experimental images, the

horizontal and vertical scales on the right hand side of the figure were chosen to fit the immobilized bottom torus. Thus, the only fitting parameter was the regularization constant ϵ in (4.5) which was chosen to be $\epsilon = 0.06$. The reason for the deviation of the scale at the top part of the experimental comparison is perspective effect due to the fact that the deflection of the real tower is not fully two-dimensional, and a small deflection of the tower in the direction normal to plane of the photograph exists.

Chapter 6

Conclusion

Solar towers have been considered in the past for many years, however, despite some of the advantages over other energy resources, there are many drawbacks for rigid towers such as the costs of the construction and repairs. To circumvent this issue, inflatable towers made out of stacked toroidal elements has been considered with the goal of reducing costs to build and maintain a solar tower. The theory for the dynamics of inflatable solar towers has been developed and numerical simulations have been performed for the two dimensional case. Experimental data has been collected and has shown to have agreement between theory and real life experiments.

Future work should include the consideration of fully three dimensional dynamics and optimal control theory by using the pressure of each individual toroidal element as a control parameter. Larger prototypes can be considered for a larger and more realistic wind profile and the data collected could used to critique the overall viability of the inflatable solar tower design. There are factors that must be taken into consideration when designing the inflatable solar towers such as the costs of the control system. For example, the power

consumption of the control system will put a constraint on the speed at which air can be pumped in and out of the tori. The efficiency of the tower should also be considered as the production of energy should be comparable to other traditional energy sources such as windmills and solar panels.

Bibliography

[Benoit et al., 2011] Benoit, S., Holm, D. D., and Putkaradze, V. (2011). Helical states of nonlocally interacting molecules and their linear stability: a geometric approach. *J. Phys. A: Math. Theor.*, 44:055201.

[Chi et al., 2014] Chi, M., Gay-Balmaz, F., Putkaradze, V., and Vorobieff, P. (2014). Dynamics and geometric control of flexible solar updraft towers. *Proceedings of the Royal Society A, under consideration*, pages 1–30.

[Ellis et al., 2010] Ellis, D., Holm, D. D., Gay-Balmaz, F., Putkaradze, V., and Ratiu, T. (2010). Geometric mechanics of flexible strands of charged molecules. *Arch. Rat. Mech. Anal.*, 197:811–902.

[Haaf et al., 1983] Haaf, W., Friedrich, K., Mayr, G., and Schlaich, J. (1983). Solar chimneys part I: Principle and construction of the pilot plant in Manzanares. *International Journal of Solar Energy*, 2(1):3–20.

[Holm, 2008] Holm, D. D. (2008). *Geometric Mechanics Part 2: Rotating, Translating and Rolling*. Imperial College Press.

[Holm and Putkaradze, 2009] Holm, D. D. and Putkaradze, V. (2009). Nonlocal orientation-dependent dynamics of charged strands and ribbons. *C. R. Acad. Sci. Paris, Sér. I: Mathematique*, 347:1093–1098.

[Mills, 2004] Mills, D. (2004). Advances in solar thermal electricity technology. *Solar Energy*, 76(1-3):19–31.

[Putkaradze et al., 2013] Putkaradze, V., Vorobieff, P., Mammoli, A., and Fahti, N. (2013). Inflatable free-standing flexible solar towers. *Solar Energy*, 98:85–98.

[Simó et al., 1988] Simó, J. C., Marsden, J. E., and Krishnaprasad, P. S. (1988). The Hamiltonian structure of nonlinear elasticity: The material and convective representations of solids, rods, and plates. *Arch. Rat. Mech. Anal*, 104:125–183.

Appendix A

Numerical codes (MATLAB)

freedynamicswind.m

```
function freedynamicswind
%Solves the differential equations for the 2D case.
%Solves boundary value problem phi(tmax)=0, p(tmax)=p0
global n p0
clear all
p0=10^5; %Atmospheric pressure in Pa
n =20; %Number of tori

k=1:2*n;
y0phi=[0.1*ones(n,1); 0*ones(n,1)];%Initial conditions for phi, dphi
tmax_free=300;
nt=200;
tspan=linspace(0,tmax_free,nt);
[t,y]=ode15s(@freedynamics,tspan,y0phi);
tfree=t;

yfree=y;
phi0=yfree(nt,1:n);
dphi0=yfree(nt,n+1:2*n);

save('./free_wind.mat','t','y');
disp('finished computation of free dynamics');

function [dU,d2U]=hderiv(x,q,r)
eps = 0.06;
```

```
h=q.*sqrt(eps^2+sin(x).^2);
dh=q.^2.*sin(2*x)./h;
d2h=q.^2.*(2*cos(2*x)./(2*h)-sin(2*x)./(2*h.^2).*dh);
dU=3./4*q.^3.*sqrt(2*r./h).*dh;
d2U=3/4*q.^3.*sqrt(2*r).*(-1/2*h.^(-3/2).*dh.^2+1./sqrt(h).*d2h);



function dy=freedynamics(t,y)
%Free dynamics of the tower
global p0 n
n=length(y)/2;

phi=y(1:n);
dphi=y(n+1:2*n);
p0=10^5; %Atmospheric pressure in Pa
r = ones(n,1); %Inner radius in m
q = 3*r; %Outer radius in m
Rspecific = 287; %Specific R for air
T = 300; %Temperature in K
rho_air = 1.2; %Density of air
p=p0*ones(n,1); %All pressures are equal
p_shift=[p0 p(1:n-1)']';
rho = p/(Rspecific*T);%Mass density
m=pi^2*rho.*r.^2.*q; %Mass of tori
I0= (5/8*r.^2 + 1/2*q.^2.*m);%Moment of Inertia

delta_phi=[diff(phi)' 0]'; %Delta phi_k
delta_phi_shift=[phi(1) diff(phi)']'; %Delta phi_k-1;

height=2*cumsum(cos(phi).*r); %The first one needs to be modified
height=height-r(1);
A=q.*(r+pi*r); %Area exposed to wind
Torque=height.*A*wind(t).^2; %Torque due to wind

[U0prime,U0dprime]=hderiv(delta_phi,q,r);
[U0prime_shift,U0dprime_shift]=hderiv(delta_phi_shift,q,r);

d2phi=(p.*U0prime-p_shift.*U0prime_shift+Torque)./(I0.*p);
```

```
dy=[dphi ; d2phi];


function U=wind(t)
U=0*sqrt(10)*sin(0.1*t/pi).^2; %Wind speed m/s
```

processdynamicswind.m

```
function processdynamicswind
%post-processing the dynamics of solar tower with wind
clf
clear all
load('./free_wind.mat','t','y'); clf
n=length(y(1,:))/2;
phi=y(:,1:n);
%plot(t,y(:,1:n));
%waitforbuttonpress
r = ones(n,1); %Sizes of tori in m
q = 3*r;
r1=[0 r(1:n-1)']';
nt=length(t);
h=(r+r1);
x=zeros(nt,n+1);
z=zeros(nt,n+1);

for k=1:nt
    x(k,2:n+1)=cumsum(h.*sin(phi(k,:)'))';
    z(k,2:n+1)=cumsum(h.*cos(phi(k,:)'))';
end
writerObj = VideoWriter('tower.avi');
open(writerObj);

set(gca,'NextPlot','replaceChildren');
for k = 1:nt
    clf

%    plot(x(k,:),z(k,:));
    hold on
    for m=1:n
        Lambda=[cos(phi(k,m)) sin(phi(k,m)); -sin(phi(k,m))
        cos(phi(k,m))];
        upvec=[0 r(m)]';
        sidevec=[q(m) 0]';
        rightup=Lambda*(upvec+sidevec);
        leftup=Lambda*(upvec-sidevec);
```

```
        x0=x(k,m+1)+[rightup(1) leftup(1)]';
        z0=z(k,m+1)+[rightup(2) leftup(2)]';
        line(x0,z0,'LineWidth',2,'Color','k');
        rightdown=Lambda*(-upvec+sidevec);
        leftdown=Lambda*(-upvec-sidevec);
        x0=x(k,m+1)+[rightdown(1) leftdown(1)]';
        z0=z(k,m+1)+[rightdown(2) leftdown(2)]';
        line(x0,z0,'LineWidth',2,'Color','k');
        sidecenter=Lambda*sidevec;

        phi0=linspace(0,2*pi,20);
        circlex=r(m)*cos(phi0);
        circley=r(m)*sin(phi0);
        plot(x(k,m+1)+sidecenter(1)+circlex,z(k,m+1)+sidecenter(2)
        +circley,'k-','LineWidth',2);
        plot(x(k,m+1)-sidecenter(1)+circlex,z(k,m+1)-sidecenter(2)
        +circley,'k-','LineWidth',2);
    end
    plot(x(k,:),z(k,:),'r-','LineWidth',1);
    set (gca,'FontSize',18);
    axis equal
    axis([-10  10 0 45]);
    hold off
    frame = getframe(gcf);
    writeVideo(writerObj,frame);
end

close(writerObj);
```